# Sensitivity of the European climate to aerosol forcing as simulated with a regional climate model

Cathy Hohenegger and Pier Luigi Vidale[1]

Institute for Atmospheric and Climate Science, Eidgenössische Technische Hochschule, Zürich, Switzerland

Received 10 August 2004; revised 26 October 2004; accepted 22 December 2004; published 18 March 2005.

[1] Despite the recognized importance of atmospheric aerosols for the simulation of present and future climate, the quantification and understanding of their impacts are still poorly constrained. Difficulties arise especially on a regional scale, owing to the short atmospheric lifetime of the aerosol particles combined with the limited observational possibilities. In this study the sensitivity of the European climate to a change in its aerosol forcing is investigated using a regional climate model (RCM) and two aerosol distributions. The original RCM aerosol climatology of Tanre et al. (1984) and a modified version of the Global Aerosol Data Set are considered, while their direct radiative forcing, together with the induced climatic response, is simulated through two five-year integrations of the RCM. The comparison of both sensitivity experiments demonstrates that the uncertainties associated with the aerosol forcing, as expressed here through the use of two different data sets, significantly influence the modeled climate on a regional scale and thus the model biases (in our case the well-known cold bias over the Iberian Peninsula and the summer dry bias over the Danube region). The observed model climatic response can be related to the modification of the radiation budget, also affecting the water cycle. The latter leads to the release of several feedbacks, i.e., cloud and water vapor feedbacks as land-atmosphere interactions, which either intensify or counteract the expected aerosol forcing, depending on the atmospheric conditions, vegetation state, and soil water content.

**Citation:** Hohenegger, C., and P. L. Vidale (2005), Sensitivity of the European climate to aerosol forcing as simulated with a regional climate model, *J. Geophys. Res.*, *110*, D06201, doi:10.1029/2004JD005335.

## 1. Introduction

[2] Atmospheric aerosols are known to influence substantially the radiation budget of the Earth through scattering and absorption (direct radiative forcing) as well as through clouds, due to their role as condensation nuclei (indirect radiative forcing). Owing to their short atmospheric lifetime, their distribution in the atmosphere shows a high variability both in space and time, which complicates the detection and the simulation of their climatic effects. As a result, the *Intergovernmental Panel on Climate Change* (*IPCC*) [2001, p. 44] stated that "obtaining accurate estimates of the aerosol forcing has been very challenging from both the observational and theoretical standpoints" and still represents a source of large uncertainty for the simulation of present and future climate.

[3] Of particular interest seems to have been the quantification of the direct radiative forcing of some aerosol species (especially soot and sulfate) on a global scale (see the review of *Haywood and Boucher* [2000]). Such estimates are obtained by interactively coupling a global circulation model (GCM) to a chemistry model or by using prescribed aerosol climatologies as input for the radiative transfer module of an atmospheric model. The derivation of the aerosol data set itself may involve results from transport chemistry models [e.g., *Tegen et al.*, 1997], emission inventories combined with Mie theory [e.g., *D'Almeida et al.*, 1991], or satellite retrievals [e.g., *Tanre et al.*, 2001; *Kaufman et al.*, 2002]. More recently, attention has been given to the response of various climate parameters (temperature, precipitation, heat fluxes, etc.) to the aerosol forcing both on a global [e.g., *Cook and Highwood*, 2004; *Wang*, 2004] and on a regional scale [*Qian and Giorgi*, 1999; *Giorgi et al.*, 2002, 2003; *Qian et al.*, 2003; *Wu et al.*, 2004]. Despite the focus of these latter studies on the eastern Asian region, they have shown evidence of the significance of the aerosol forcing on a range of climate parameters relative to a climate containing no aerosol.

[4] Even so, many atmospheric models still use old and coarse data sets to account for the radiative properties of the aerosol particles. A climatology widely implemented both in numerical weather prediction (e.g., in the Lokal Modell in use in Germany, Switzerland, Italy, Greece, and Poland) and climate models (e.g., the Climate High-Resolution Model [*Vidale et al.*, 2003], the ARPEGE-Climat GCM [*Hu et al.*, 2001]) was derived back in the year 1984 by *Tanre et al.*

[1]Now at National Environment Research Council Centres for Atmospheric Science, Centre for Global Atmospheric Modeling, University of Reading, Reading, UK.


0148-0227/05/2004JD005335$09.00

[1984]. Even if such RCMs were not primarily intended for the study of the climatic effects due to the aerosol particles, they are used to simulate present and future climate and to assess climatic changes. In that optic, the impacts of the uncertainties generally associated with the radiative forcing of the aerosol species [e.g., *IPCC*, 2001] on the simulated precipitation or temperature field over a region are not clear a priori.

[5] The goal of this study is to explain the response of simulated regional climate to a change in the radiative forcing of its aerosol particles and, as a consequence, to understand how aerosols should be consistently specified in a RCM. Our methodology involves contrasting the results of two simulations performed with a RCM driven by perfect boundary conditions and using two different prescribed aerosol climatologies. The use of a RCM driven by perfect boundary conditions has two advantages. First, it provides very constrained conditions, reducing the degrees of freedom, simplifying the interpretation and allowing in the analysis the differentiation between the climatic effects due to the radiative properties of the aerosols and those induced by feedback processes. Second, since the chosen RCM has already been extensively tested, validated and intercompared [see *Vidale et al.*, 2003; *Frei et al.*, 2003; *Hagemann et al.*, 2004], its main climatic patterns, its biases and uncertainties are well-known features. We can thus concentrate on the significance of the obtained sensitivity, which will be assessed against observations and known model biases whenever relevant. The main limitation of this particular modeling tool is that its radiative transfer scheme [*Ritter and Geleyn*, 1992] requires prescribed aerosol climatologies and cannot be used for the simulation of the aerosol indirect radiative forcing.

[6] The chosen RCM is the Climate High-Resolution Model (CHRM), driven at its boundaries by ERA-15 data [*Gibson et al.*, 1997]. The first aerosol data set considered is the original RCM aerosol climatology based on the work of *Tanre et al.* [1984], while the second one corresponds to a modified version of the Global Aerosol Data Set [*Hess et al.*, 1998]. They account for the contribution of aerosol particles produced both anthropogenically (e.g., soot, sulfate) and naturally (e.g., dust, sea salt).

[7] The structure of the paper is as follows. Section 2 describes the methodology and especially the characteristics of the CHRM model, of the considered aerosol distributions and of the sensitivity experiments. The presentation of the results follows in term of the changes induced in the radiation components, in the temperature and precipitation fields and in the surface fluxes. The responsible mechanisms and the overall climatic sensitivity are discussed in section 4 while conclusions are given in section 5.

## 2. Method

### 2.1. Climate High-Resolution Model

[8] The Climate High-Resolution Model (CHRM) version 2.3 [see *Vidale et al.*, 2003] is a state of the art regional climate model, using a regular latitude/longitude grid (0.5° by 0.5°) with a rotated pole and a hybrid sigma pressure coordinate. This RCM is based on the mesoscale weather forecasting model of the German and Swiss meteorological services [*Majewski*, 1991; *Majewski and Schrodin*, 1994] but was adapted for climatic applications. Its physical package includes a mass flux scheme for convection [*Tiedtke*, 1989], Kessler-type microphysics [*Kessler*, 1969; *Lin et al.*, 1983], a land surface scheme [*Dickinson*, 1984], and a soil thermal model [*Jacobsen and Heise*, 1982]. Vertical diffusion and turbulent fluxes in the atmosphere are parameterized by a flux gradient approach (of the *Beljaars and Viterbo* [1998] type in the surface layer and *Mellor and Yamada* [1974] type in the boundary layer). The CHRM model also includes a radiative transfer scheme developed by *Ritter and Geleyn* [1992]. The latter is based on the solution of the delta-two stream version of the radiative transfer equation allowing in each model layer scattering, absorption and emission of radiation in eight spectral intervals (three shortwave and five longwave bands) by cloud droplets, aerosols, and gases ($H_2O$, $O_3$ and a composite gas made of $CO_2$, CO, $O_2$, $CH_4$ and $N_2O$). The minimal aerosol parameters needed by the Ritter and Geleyn radiative transfer scheme are spectrally averaged 3-D fields of the optical depth (integral of the extinction coefficient between two model levels), of the single scattering albedo and of the asymmetry parameter.

### 2.2. Specification of the Aerosol Distribution

#### 2.2.1. *Tanre et al.* [1984]

[9] The aerosol climatology originally implemented in the CHRM model was created by D. Tanre, J. F. Geleyn, and J. Slingo in 1984 [*Tanre et al.*, 1984] using the recommendations of the *World Climate Research Program* [1980]. Urban, maritime, land, desert, tropospheric background, stratospheric background, and volcanic aerosols are defined on a T10 spectral distribution in which the last three classes are prescribed as horizontally homogeneous. Vertically, each aerosol component is associated with a height profile, assuming an exponential decay of the aerosol concentration through the troposphere or through the stratosphere for the stratospheric and volcanic backgrounds. Their distribution is fixed in time and their optical properties do not vary with relative humidity.

[10] Figure 1 shows the optical depth at 0.55 μm of the tropospheric aerosols (sum of urban, maritime, land and desert classes) and of the desert component solely. Tanre's distribution is characterized by large-scale patterns with smooth symmetrical structure, a result of its spatial resolution designed for use in a low resolution global climate model of the year 1984. The comparison of the total aerosol optical depth with the optical depth of the desert class further reveals the dominance of the desert component. This is true even over Europe, where man-made aerosols (of the type in the urban class) would have been rather expected (see, e.g., Figure 2).

#### 2.2.2. GADS Data Set

[11] The Global Aerosol Data Set (GADS; *Hess et al.* [1998]) is based on the work of *D'Almeida et al.* [1991] using emission inventories and Mie theory to compute the different aerosol distributions and optical properties. It provides particle number densities and several optical properties for a set of wavelengths, relative humidities (0, 50, 60, 70, 80, 90, 95, 98, and 99%) and components on a 5° by 5° latitude/longitude grid and for two time periods (March–August and September–February). Those include soot, insoluble, water-soluble, mineral, sea salt,

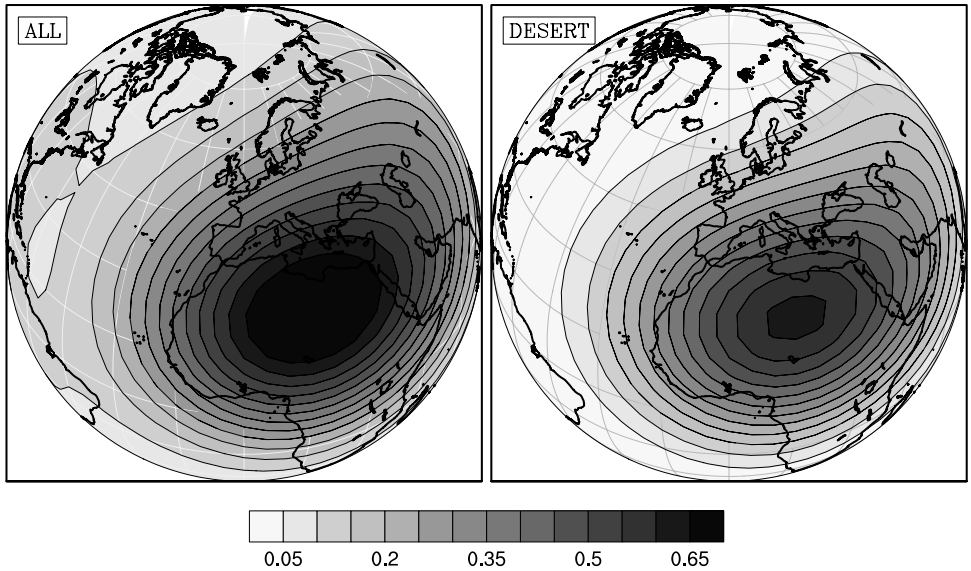


**Figure 1.** Aerosol optical depth at 0.55 μm derived from Tanre's data set with (left) the sum of the urban, maritime, land, and desert classes and (right) the desert component.

sulfate (75% $H_2SO_4$ produced over the Antarctic), tropospheric background, and stratospheric background. Their concentration varies both horizontally and vertically except for the background aerosols which are set at a fixed value in the horizontal plane.

[12] Figure 2 shows the yearly mean of the aerosol optical depth at 0.55 μm for the GADS data (by a relative humidity of 80%) beside the one retrieved by the Moderate Resolution Imaging Spectroradiometer (MODIS) satellite [*Kaufman et al.*, 2002]. In contrast to Tanre's climatology, the GADS data set shows two distinct types of maximum, the first one associated with the production of desert dust (as over the Sahara) and the second one with the emission of anthropogenic aerosols over polluted area (as over Europe). This behavior seems to be in better agreement with the MODIS data, even if their agreement is far from being perfect. Their discrepancy follows from the characteristics of both the GADS data set and the MODIS data, in particular: use of Mie theory and "older" emission inventories by GADS; problematic retrieval of the optical depth over land, short measurement period (2000–2001) and no retrieval at high latitudes, over deserts, and on cloudy days by MODIS.

[13] For the implementation of the GADS data in the CHRM model, some adaptations were introduced. They aim to find a compromise between a still "realistic" aerosol distribution, CHRM characteristics (e.g., high resolution), GADS characteristics and computing efficiency. The most important changes consist in the introduction of an aerosol distribution invariant with time and with relative humidity.

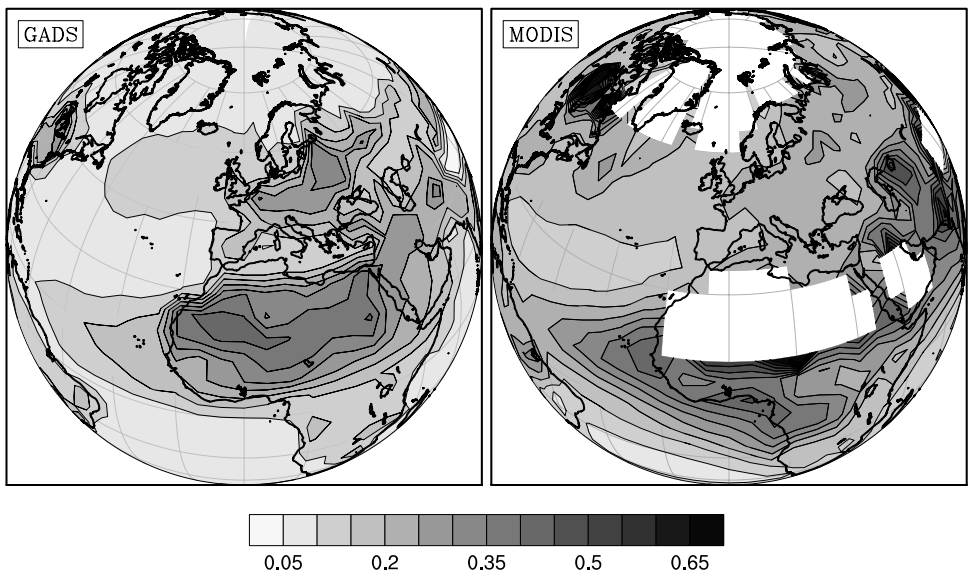


**Figure 2.** Yearly mean of the aerosol optical depth at 0.55 μm derived from (left) the GADS data set and (right) from MODIS.

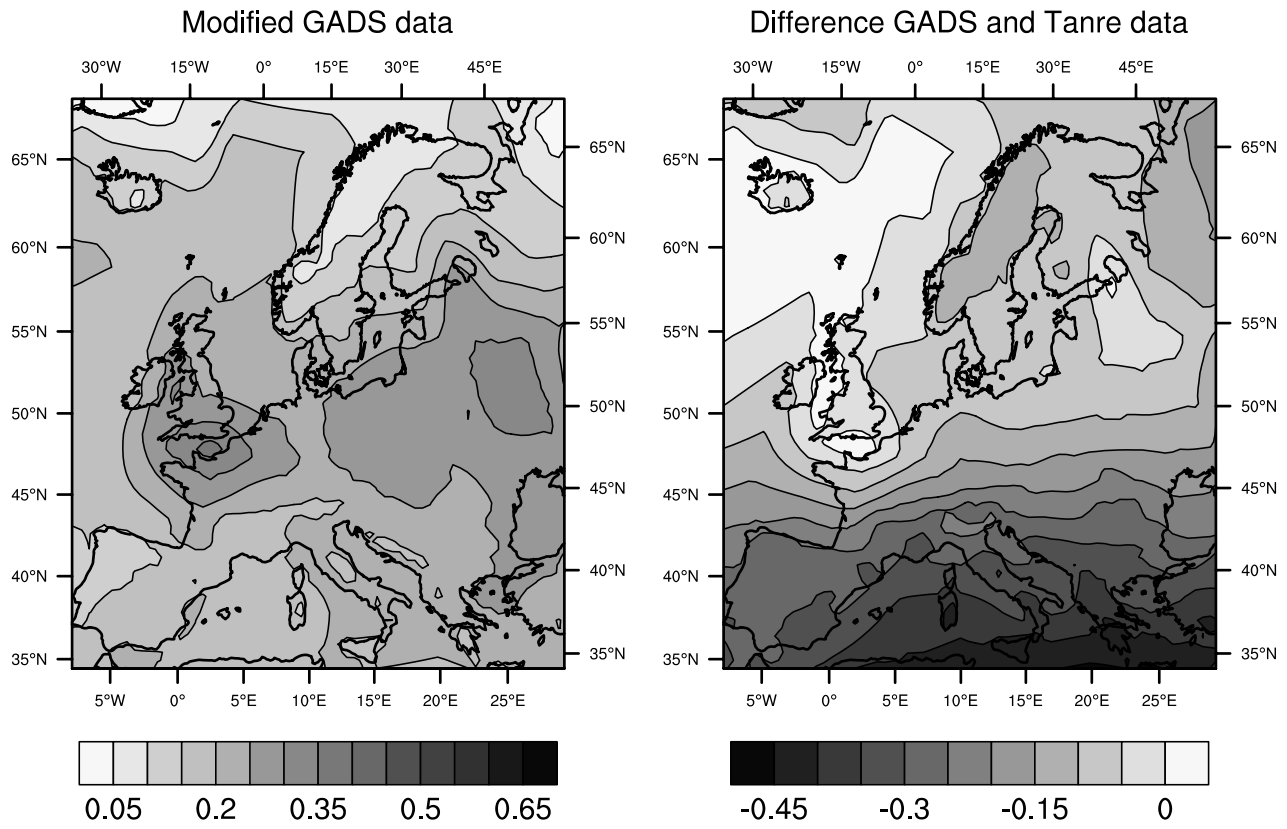


**Figure 3.** Aerosol optical depth at 0.55 μm of (left) the modified GADS data set interpolated on the model grid and (right) its difference to Tanre's climatology.

The first choice is justified by the crude resolution of the aerosol seasonal cycle in the GADS data set and the second one by the few resulting combination possibilities between the nine humidity classes in GADS and the limited variability of the relative humidity within CHRM for the chosen domain. For example, in order to cover the variability of the simulated relative humidity over Europe, only the three classes 70%, 80%, and 90% of the GADS data would be used. Since the 70% and 80% values are quite similar, the degrees of freedom mainly reduce to two, with a predominance of the 80% values. Only these last ones were thus considered. In the vertical, the height profiles were also smoothed at the different boundaries of the aerosol layers to avoid undesirable effects on the model dynamics.

[14] The resulting distribution, interpolated on the CHRM domain, is shown on Figure 3, with its difference to the Tanre data. The maximum appearing over the British Channel is slightly artificial since it results from the regridding transformation. Main features are, in comparison to Tanre's data set, the removal of a very zonal aerosol distribution, a smaller extent of the aerosols in the vertical (not shown), and the overall reduction of the optical depth on the continents. As a consequence, the new aerosol climatology will both scatter and absorb less radiation than the older one in the shortwave and longwave range. The reduction of the shortwave absorption follows here despite the transformation from dust-like (more scattering) to pollution-made aerosols (more absorbing) since the higher particle number density of the dust particles in Tanre, as compared to the soot component in GADS, more than compensates for their smaller normalized absorption coefficient. The uncertainties associated with this new distribution are rather related to the difficulty in finding aerosol climatologies fulfilling the requirements of a RCM and to the characteristics of the original GADS data, rather than to the undertaken simplifications.

### 2.3. Experimental Design

[15] In order to test the sensitivity of the European climate to different aerosol forcings, two experiments were performed with alternative aerosol representations. The first one (CTL) uses the distribution derived by *Tanre et al.* [1984], replaced in the second experiment (GADSN) by the modified GADS data set. The surface boundary conditions were imposed by the monthly ISLSCP I [*Sellers et al.*, 1994] climatology, while ERA-15 data were used as lateral boundary conditions and to drive the sea surface temperature. Both simulations were integrated over a standard European domain (see Figure 4), also used in other studies [e.g., *Vidale et al.*, 2003], with 20 layers in the vertical and 3 layers in the soil. Each integration was started from 1 January 1979 for a period of 5 years with a time step of 5 min and a 1.5 hour radiation call. Five years were deemed appropriate in order to avoid spurious effects resulting from the identical initial conditions combined with long-term memory effects (for example those associated with soil moisture, see section 4.1).

### 2.4. Observations

[16] Observations used to assess the significance of the differences obtained between the two simulations were

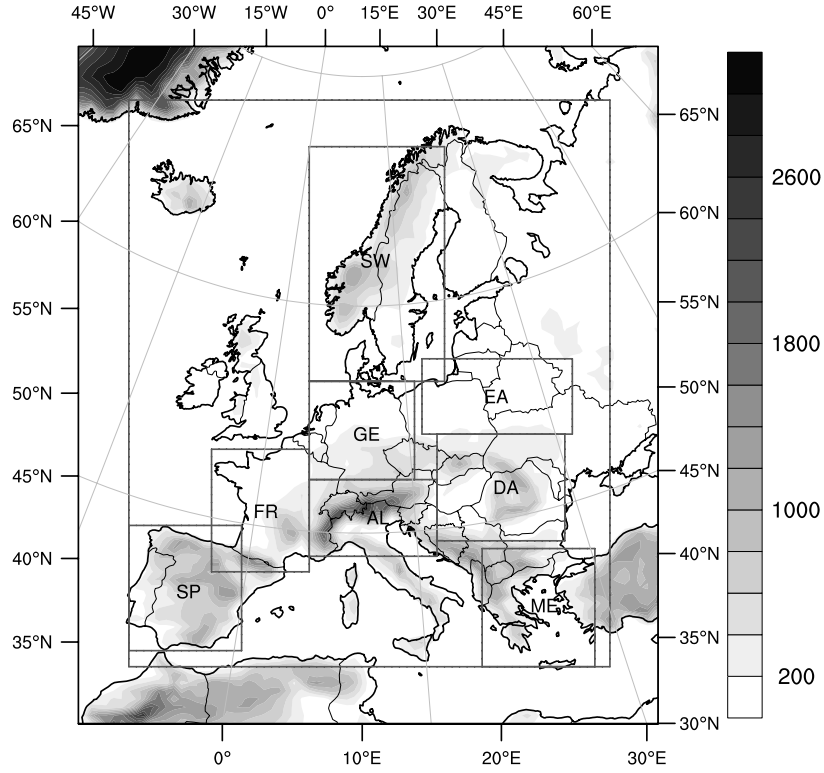


**Figure 4.** The CHRM domain (EM) and subdomains [after *Vidale et al.*, 2003]. AL stands for Alpine region, DA for Danube catchment, EA for east Europe, FR for France, GE for Germany, ME for southeast Mediterranean, SP for Spain (Iberian Peninsula), and SW for Sweden (Scandinavia).

extracted from the Climatic Research Unit (CRU) data set [*New et al.*, 1999], which provides among other elements precipitation and temperature data over land at 50 km resolution. For the validation of the simulated solar fluxes, measurements collected at the Automatisches Messnetz (ANETZ) stations of MeteoSwiss were used. They were preferred to a global database like the Global Energy Balance Archive (GEBA) [*Gilgen et al.*, 1998] despite their limited spatial and temporal extent (i.e., over Switzerland and over the period 1981–1983) for two reasons. First, they show a much higher density than the GEBA data with 72 stations over Switzerland against 1 and are present both over mountainous and flat terrains. Second, even if cloud observations were not directly available in either data set, they offer the possibility to derive approximated values for the incoming radiation under clear-sky condition by using the measurements of the sunshine duration to distinguish cloudy from clear sky.

## 3. Results

[17] Previous integrations with the CHRM model [see *Frei et al.*, 2003; *Vidale et al.*, 2003] have shown that the CHRM model has skill in representing the European mean climate and its associated interannual variability in precipitation and surface temperature. More precisely, the control CHRM model version is able to simulate over most part of the European domain solar radiation within at most 5 W/m$^2$ (15 W/m$^2$) in winter (summer), temperature within at most 2°C and precipitation within 1 mm/day. Since the CTL and GADSN simulations show very similar basic climatic features, where the mean patterns of the control experiment can be found in the work of *Vidale et al.* [2003], we concentrate here on the differences obtained between both simulations for a range of climate parameters.

### 3.1. Radiation

[18] Figure 5 shows maps of the 5-year mean difference obtained in the net solar flux both at the Earth's surface and at the top of the atmosphere in winter and in summer. The differences are expressed as deviations from the control simulation. The use of the GADS aerosols, instead of the ones in Tanre, leads to an increased surface net shortwave flux, except over some northern places in summer (Scotland and part of Scandinavia). Characteristic is the strong meridional gradient with a south to north decrease of the radiative forcing. The differences are, as expected, more pronounced in summer amounting to 12.7 W/m$^2$ (domain average) against 5 W/m$^2$ in winter.

[19] At the top of the atmosphere (see Figure 5), simulation GADSN shows a reduced net solar flux except over the southern part of the EM domain. The mean forcing is an order of magnitude smaller than at the Earth's surface with $-0.39$ W/m$^2$ in winter (domain average) and $-2.97$ W/m$^2$ in summer. In winter the largest negative values are found over the Alps, while in summer they merely coincide with the minima in the surface net solar flux.

[20] Since the forcing values obtained at the top of the atmosphere do not compensate the ones observed at the Earth's surface (see Figure 5), a different portion of the solar radiation must be absorbed within the atmosphere between both simulations. The corresponding maps

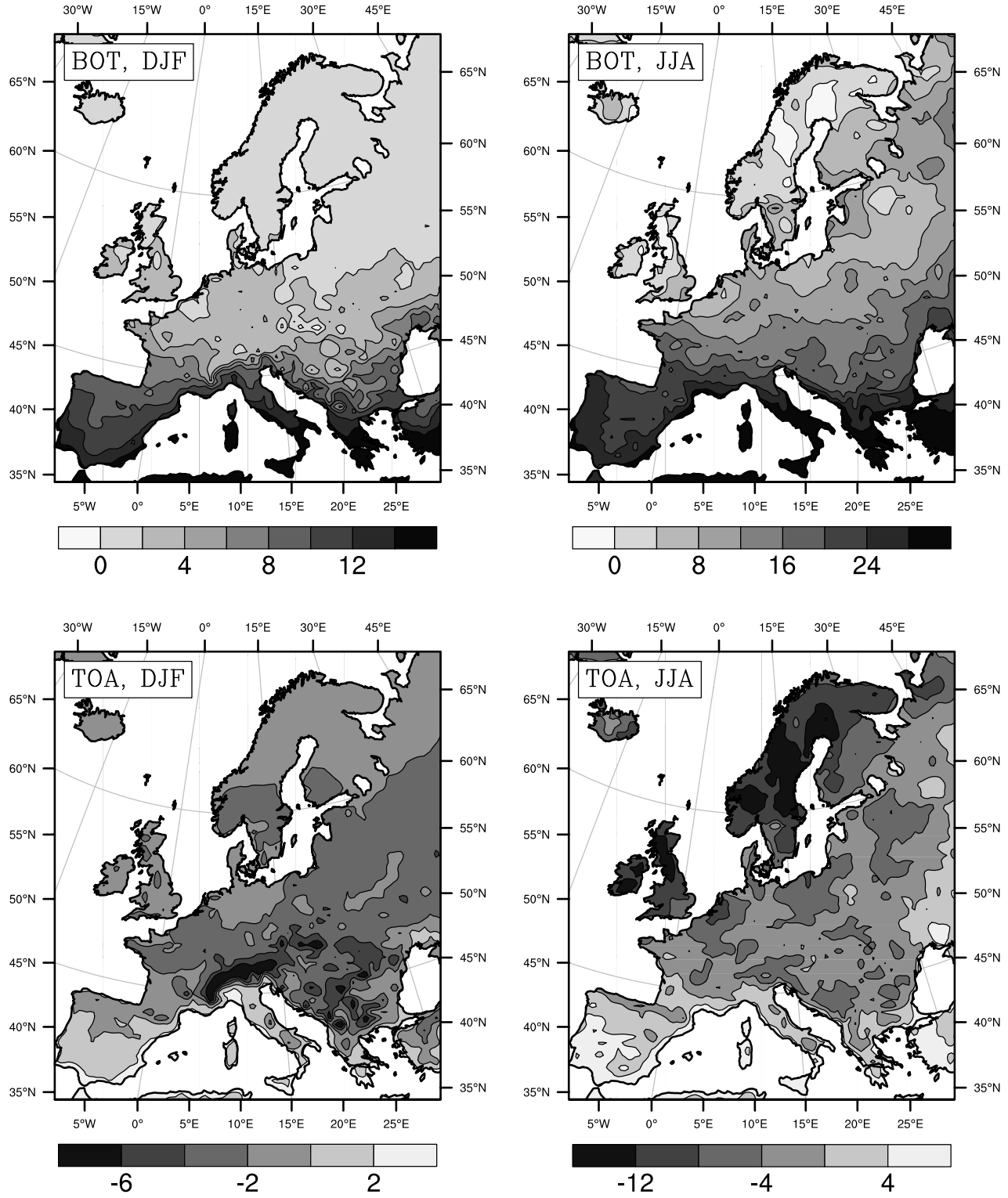


**Figure 5.** Difference (GADSN-CTL) in the net solar flux (W/m$^2$) at the surface (BOT) and at the top of the atmosphere (TOA) averaged over winter (DJF) and summer (JJA).

(not shown) reveal an overall weaker absorption of the solar radiation by the new aerosols both in winter and summer, where the differences are aligned along a strong meridional gradient. Values range from $-15$ to 0 W/m$^2$ in winter (from south to north) and from $-30$ to $-5$ W/m$^2$ in summer.

[21] Figure 6 illustrates the corresponding summer time picture for the net longwave flux. The winter situation is not shown due to the small differences encountered ($\pm 1$ W/m$^2$ except over southern Europe). At the Earth's surface the GADS climatology leads to an enhanced emission of terrestrial radiation and/or reduced atmospheric emissions

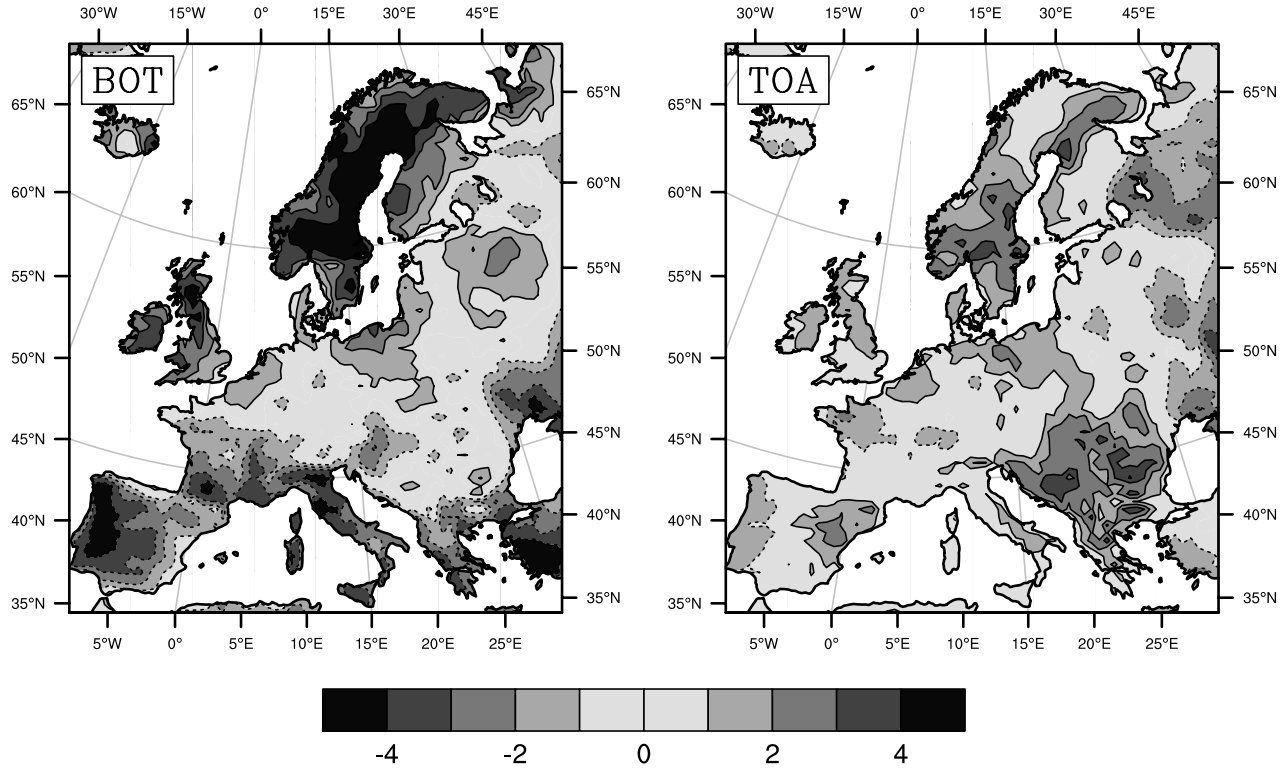


**Figure 6.** Summer difference (GADSN-CTL) in the net longwave flux (W/m$^2$) at the surface (BOT) and at the top of the atmosphere (TOA). Positive contour lines are continuous, negative ones are dashed.

over the southern countries (negative values). The opposite situation occurs over the northern regions with an extended maximum over Scandinavia. At the top of the atmosphere the response is rather moderate (±2 W/m$^2$) except for the maxima appearing over the Danube region and over southern Scandinavia.

[22] Since the obtained 5 and 12.7 W/m$^2$ as mean forcing for the net shortwave flux at the Earth's surface in GADSN correspond well in location and magnitude to known CHRM biases of up to 5 and 15 W/m$^2$, their significance in terms of model biases is further analyzed with Figure 7 (see also sections 2.4 and 4.2). Figure 7 contrasts the simulations of the incoming radiation and of the incoming radiation under clear sky (to avoid the compensation of model errors, see section 4.2) with the corresponding ANETZ observations for the period 1981–1983 and for two grid boxes taken over Switzerland. The first one (top) is situated over the Alps, the second one (bottom) over the Swiss Plateau in a relatively flat area, and both of them are characteristic examples for these two regions. The clear-sky radiation was obtained by fitting a Gaussian curve through the simulated or measured incoming radiation on cloudless days (i.e., the squares on Figure 7). Cloudy and cloudless days were differentiated by means of thresholds based on the simulated cloud cover (for the GADSN and CTL curves) and on the hourly measurements of the sunshine duration (for the ANETZ curve).

[23] Over both regions and independently of the presence of clouds, simulation GADSN exhibits a larger incoming radiation than CTL, in agreement with Figure 5. When clouds are filtered, it becomes more apparent that the GADSN curve tends to cross the observational curve, particularly over mountainous regions. This is caused by a slight underestimation of its incoming radiation in winter followed by an overestimation in summer. Correspondingly, simulation CTL shows a pronounced underestimation of its clear-sky incoming radiation during the cold months and either a slight overestimation or underestimation in summer.

### 3.2. Temperature and Precipitation

[24] Figure 8 shows the 5-year mean difference induced in the temperature field in winter and summer for the period 1979–1983. The winter map points to a warming in simulation GADSN over southern Europe and rather moderate cooling/warming over the remaining regions. In summer, only the southern countries Spain, Italy, Greece, Turkey, and parts of France show increased values of the temperature in GADSN relative to CTL. This latter peaks at 0.8°C over Spain against −0.5°C over northeastern Europe. The forcing values observed in summer are also larger than in winter and may be especially of opposite sign. Clear examples are Denmark and southern Scandinavia, parts of northeastern Europe or the western coast of the Black Sea which switch between warming in winter and cooling in summer. Since we are using invariant aerosol distributions, this behavior is unequivocally a sign for the presence of feedbacks, which can counteract the expected aerosol forcing (see section 4.1).

[25] The significance of the temperature changes obtained between the simulations is assessed with Figure 9, which shows the temperature bias calculated as deviation from CRU data for the 1979–1983 period and averaged over winter and summer time. In winter, both simulations show similar biases except over the southern countries and

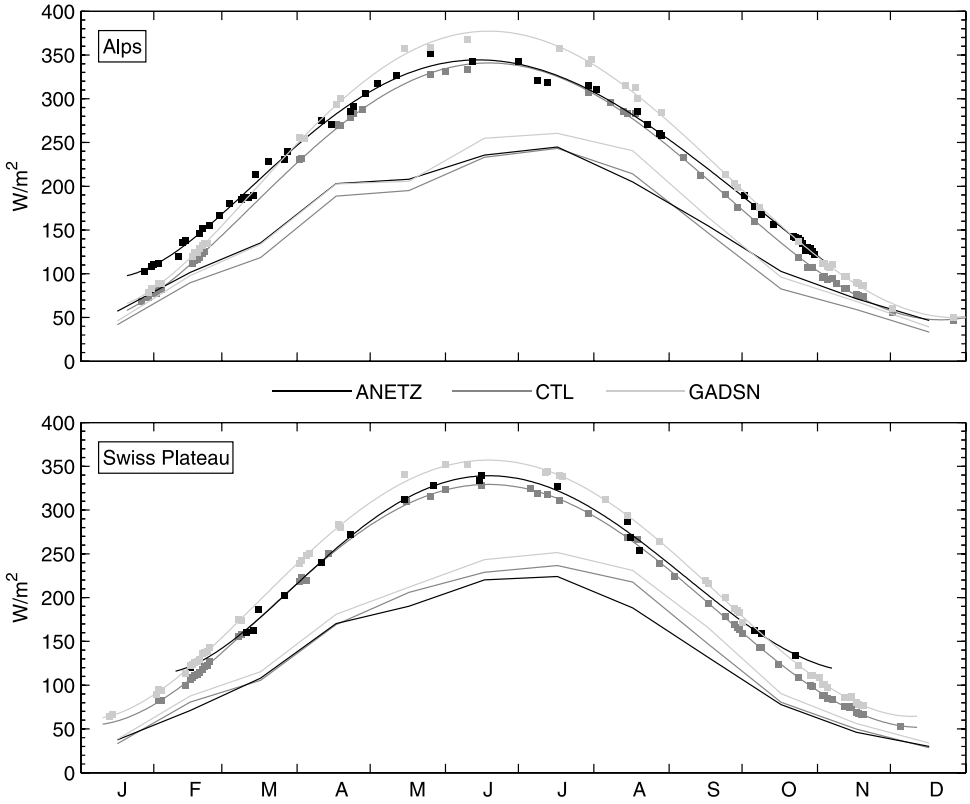


**Figure 7.** Yearly cycle of the incoming radiation (averaged over 1981–1983, monthly values, solid lines) and incoming radiation under clear sky (squares with the corresponding fitted Gaussian curves) in $W/m^2$ for the two simulations (GADSN, CTL) and the ANETZ observations of MeteoSwiss.

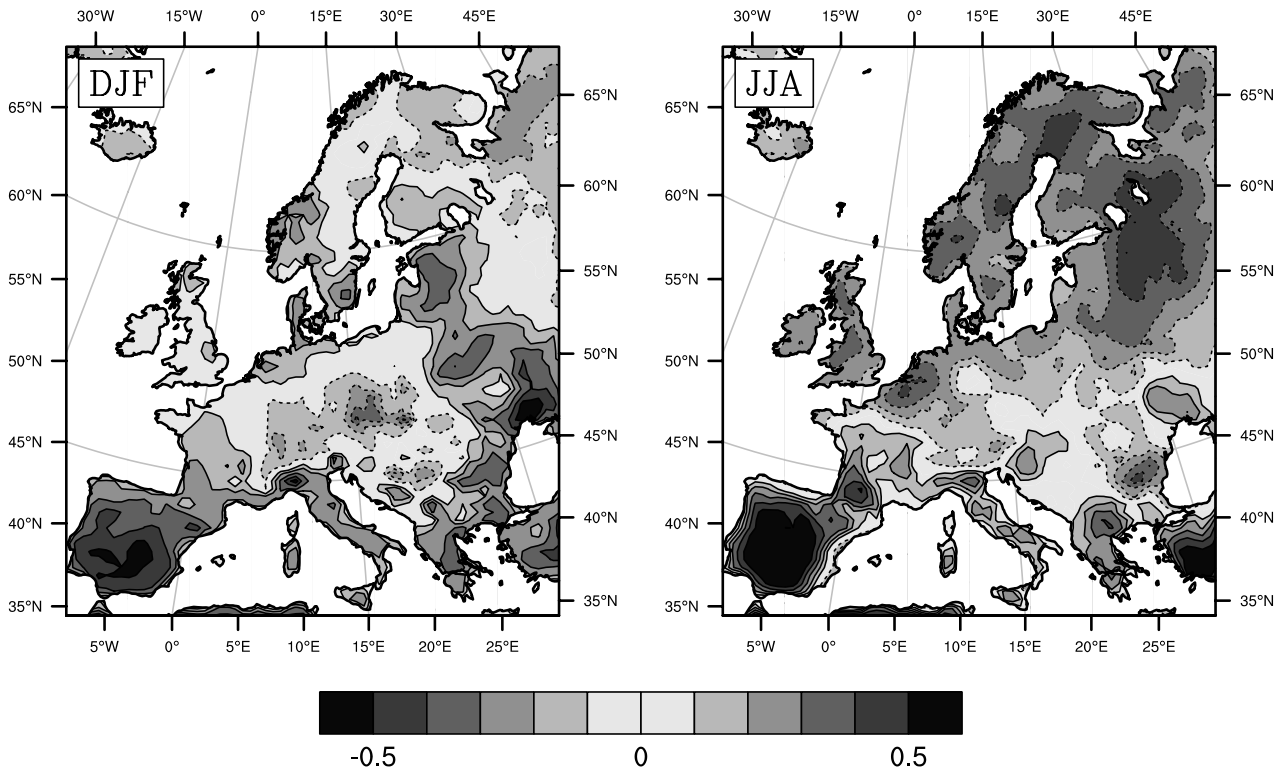


**Figure 8.** Temperature difference (GADSN-CTL; in degrees Celsius) averaged over winter (DJF) and summer (JJA). Positive contour lines are continuous, negative ones are dashed.

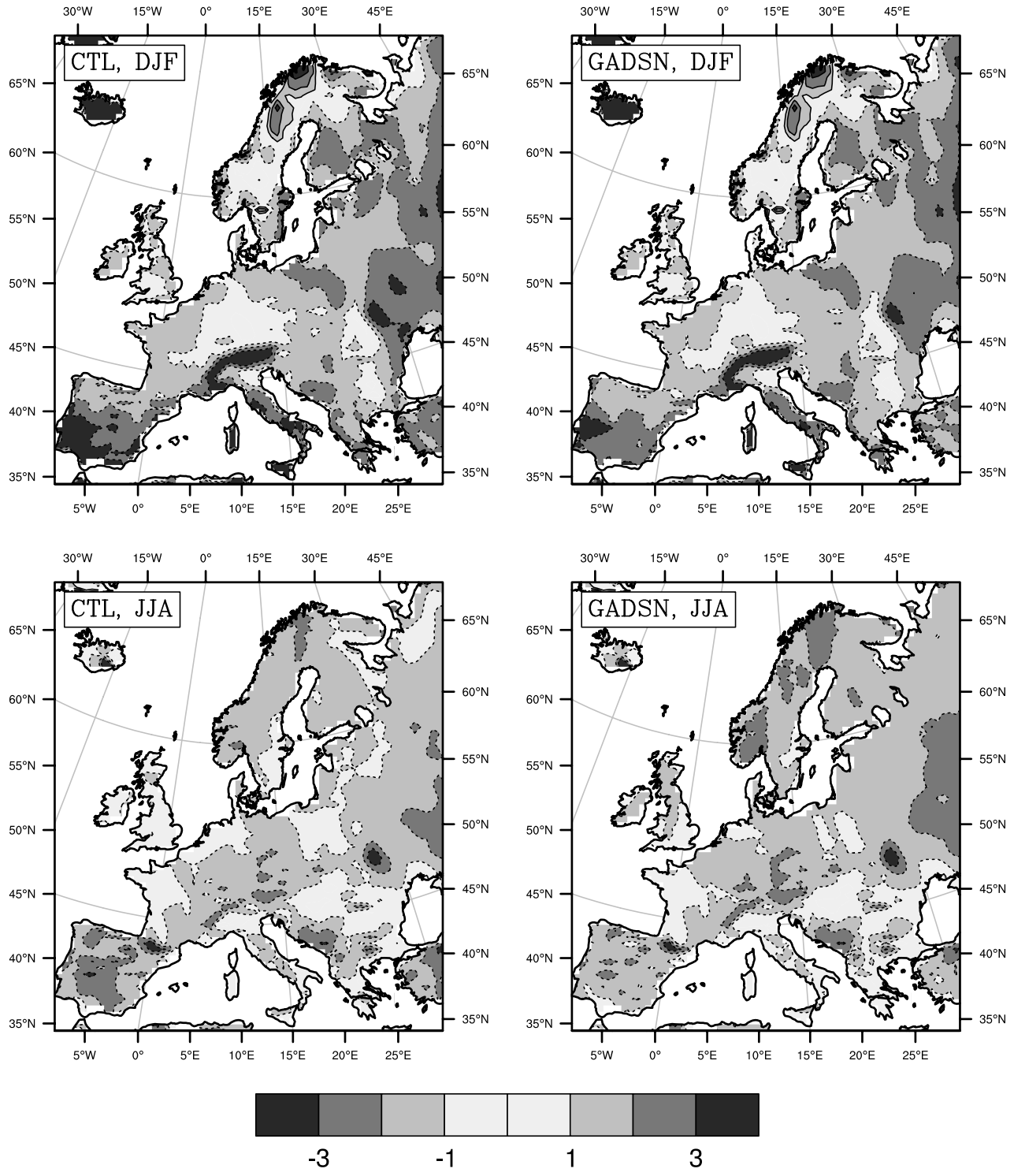


**Figure 9.** Temperature bias (°C) of the simulations CTL and GADSN relative to the CRU data for winter (DJF) and summer (JJA). Negative contour lines are dashed, positive ones are continuous.

especially over Spain, i.e., the temperature response to the modification of the aerosol representation can not be seen as significantly over central and northern Europe. In summer, both the warming obtained in GADSN over Spain (with respect to CTL) and the cooling over Scandinavia and part of northeastern Europe are large enough to affect the model biases. Since *Vidale et al.* [2003] have shown that the CHRM model has a tendency to be especially cold over Spain with a mean bias in the order of −2°C, the warming of about 0.5°C induced by the new aerosol distribution is noteworthy.

[26] Figure 10 shows the annual mean summer difference in convective precipitation obtained between simulations GADSN and CTL for the domains defined in Figure 4.

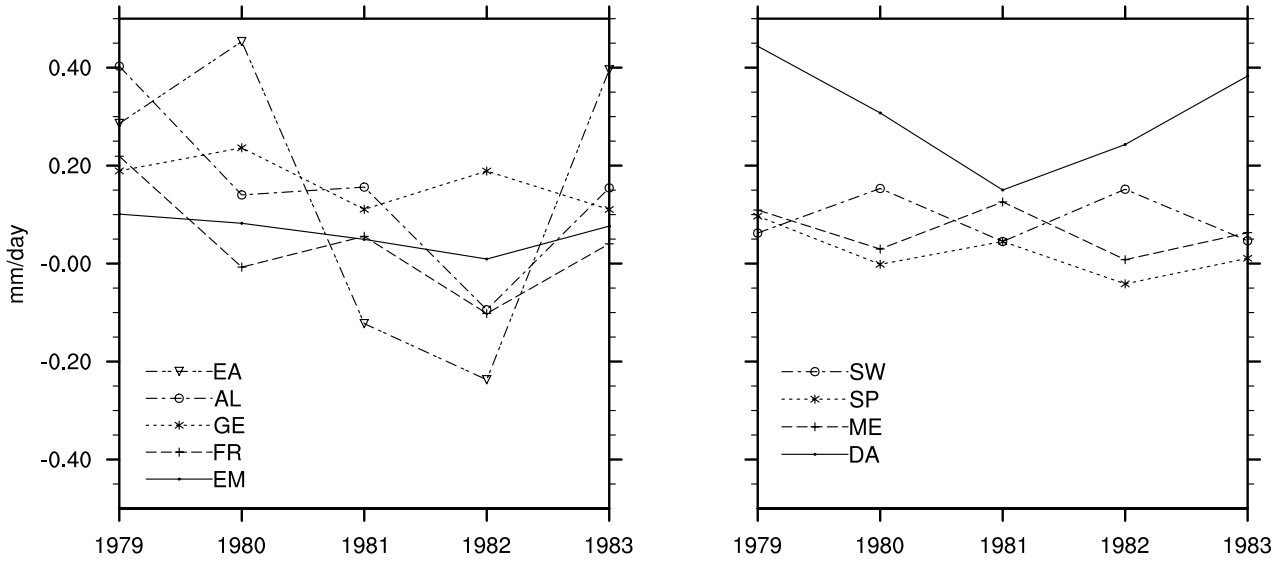


**Figure 10.** Summer difference in the convective rain in millimeters per day from 1979 to 1983 averaged over the domains defined on Figure 4.

In winter, as for stratiform rain and snow, no significant change could be observed. Figure 10 highlights a generally increased convective activity in simulation GADSN, even if a certain spatial and temporal variability is present. The Danube catchment especially receives a surplus of 0.4 mm/day in the first year what compensates a part of its well-known dry bias of about 1.2 mm/day [see, e.g., *Vidale et al.*, 2003]. The 5-year mean winter and summer deviation of the simulated precipitation from CRU observations is illustrated in Figure 11. Comparison of the left and right maps on Figure 11 confirms that the new aerosol distribution induces a significant precipitation increase in summer over the Danube region, as well as over northeastern Europe.

### 3.3. Surface Fluxes and Soil Moisture

[27] Since the surface and water fluxes affect temperature and precipitation, their response to the modified aerosol distribution, expressed by different radiation budgets between simulations GADSN and CTL (see section 3.1), is illustrated with Figure 12. Figure 12 shows the 5-year mean difference in the sensible and latent heat fluxes averaged over summer time. The winter situation displays a similar pattern, albeit with smaller values. According to the large increase of the surface net solar flux in GADSN, pronounced differences can be observed with maxima around 30 W/m$^2$ for the sensible heat flux and 20 W/m$^2$ for the latent heat flux. The comparison of the left and of the right map on Figure 12 shows a correspondence between the response of the sensible and latent heat fluxes: The latter is larger in simulation GADSN over the midlatitude (except France) and northern domains where the sensible heat flux tends to decrease compared to CTL. In contrast, France and the southern countries show a strong warming associated with a moderate drying.

[28] To further illustrate the interplay between the heat and water fluxes, we consider Figure 13. Figure 13 shows the yearly cycle of the latent heat flux, sensible heat flux, and soil moisture averaged over Spain and over the Danube region for the year 1979. Spain is representative of the southern domains, the Danube catchment depicts the situation met over most other regions, and the consideration of the soil moisture evolution is dictated by its relation to the latent heat flux. Figure 13 shows an overall depletion of the soil moisture in simulation GADSN compared to CTL. Over Spain the drying of the soil already begins in February and is much more pronounced than over the Danube catchment. The observed reduction in the soil water content can be interpreted as the result of the increased latent heat flux; its severe depletion over Spain seems to strongly limit the evapotranspiration in late summer, thus favoring an increase of sensible heat flux (see also section 4.1). Since the depletion mostly affects the root zone (not shown), the extra latent heat flux obtained in simulation GADSN is mainly due to an enhanced plant transpiration. This holds even if the minimum in the soil water content appears between 3 and 4 months after the maximum in the evapotranspiration. Indeed, as long as the balance between precipitation, evapotranspiration and runoff does not become positive, the soil will keep on losing water (cumulative effect).

## 4. Discussion

### 4.1. Mechanisms and Feedbacks

[29] Several mechanisms are responsible for the climatic response presented in section 3. The increase of the net solar flux at the surface and the reduction of its absorption in the atmosphere in simulation GADSN primarily follow from the smaller optical depth and absorption coefficient of the GADS aerosols. The observed meridional gradient, a common feature to Figures 3 and 5, is a good illustration of it. This behavior is strengthened by the meridional nature of the solar flux slightly modified by the surface albedo (e.g., over the snow covered regions in winter). In short, the amount of originally available radiation and the changes imposed on the original aerosol climatology almost explain on a one-to-one basis the forcing obtained at the Earth's

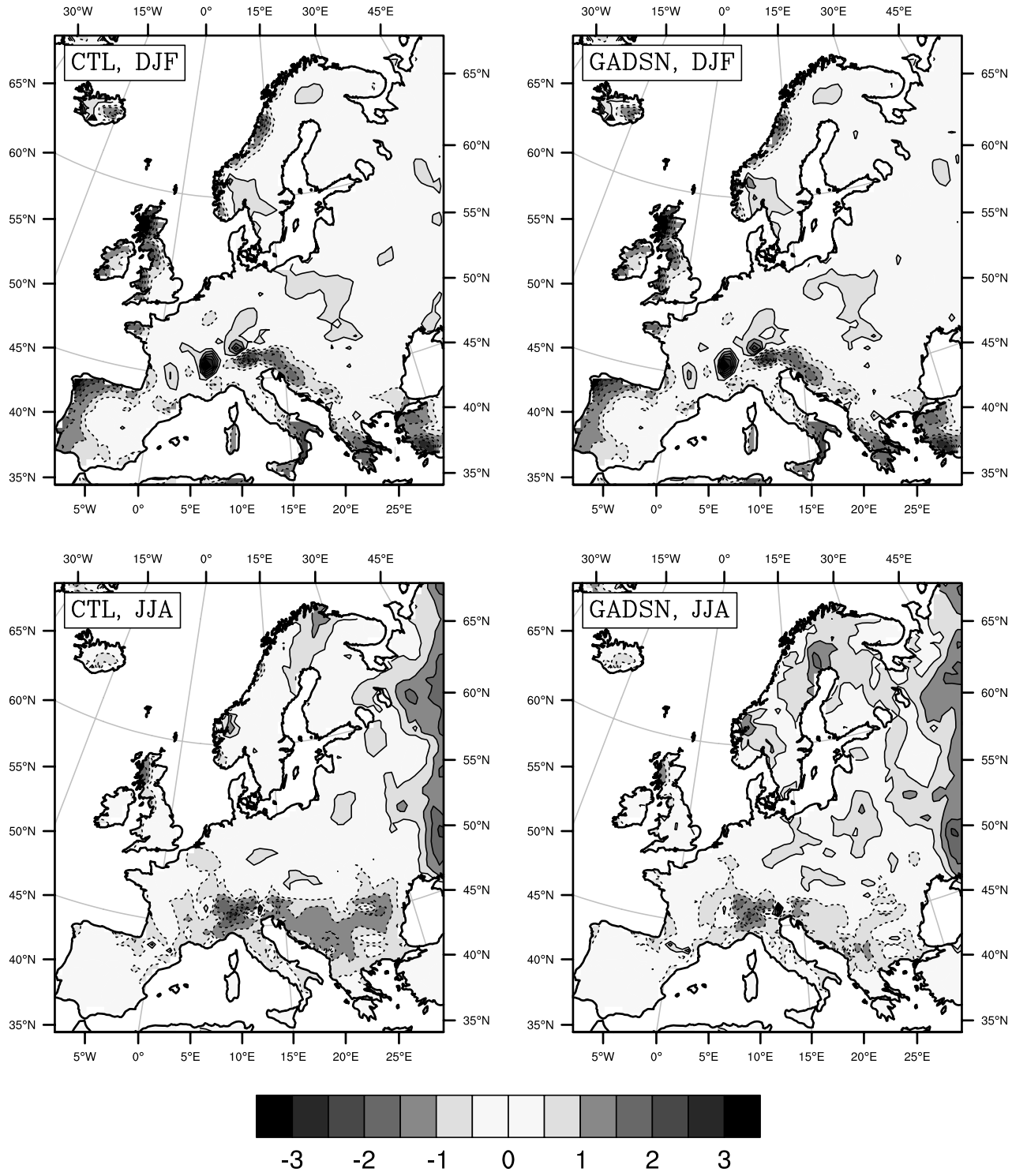


**Figure 11.** As in Figure 9, but for precipitation (in millimeters per day).

surface, in the atmosphere, and as a consequence, at the top of the atmosphere. Calculated correlations between them yield 0.95 (0.90) in winter (summer) for the forcing values induced at the Earth's surface and 0.99 (0.96) for the solar flux absorbed within the atmosphere. The slight decrease of the correlation coefficient in summer is noteworthy and indicates the inclusion of water vapor and cloud feedbacks impacting on the radiation budget, as further detailed below.

[30] In the longwave range the direct effects of the aerosols cannot be distinguished from those mediated by subsequent surface temperature and cloud changes, owing to their smaller optical depth. Changes in the cloud cover are especially responsible for the maxima observed in the longwave range in Figure 6, both at the Earth's surface and at the top of the atmosphere. The increased values of the surface net solar flux obtained in simulation GADSN

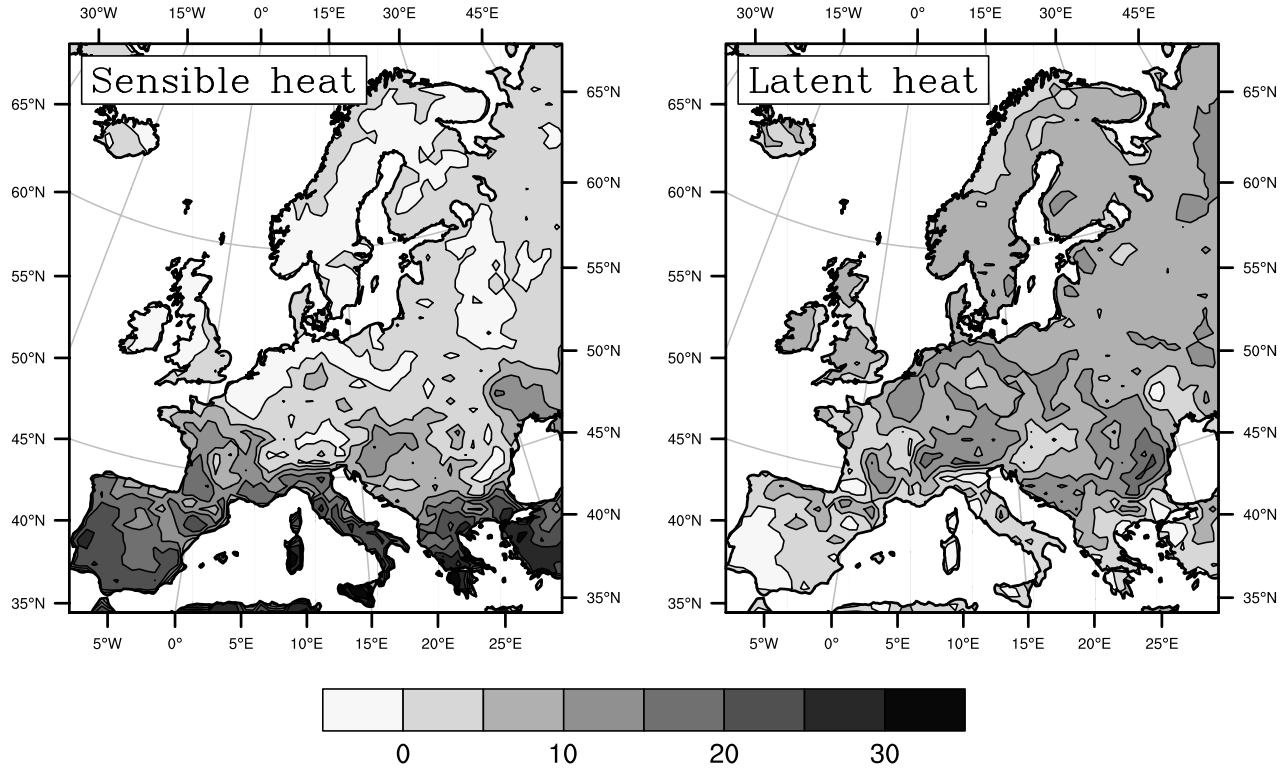


**Figure 12.** Difference ($W/m^2$) between GADSN and CTL obtained for (left) the sensible heat flux and for (right) the latent heat flux.

compared to CTL can lead here to warmer temperatures, enhanced terrestrial emissions, and sensible heat fluxes. This typically happens over the southern countries Italy, Greece, Turkey, and Spain and generally over the whole European domain in winter. However, an enhanced evapotranspiration accompanied by a slight cooling tendency and by increased water vapor and cloud feedbacks can supply the expected warming, as found, for example, over the Danube region in summer. This dual behavior in the partitioning of the extra net solar flux between sensible and latent heat flux is best revealed during the adjustment period (1979), when the climatic system tries to balance itself between the following two pathways.

#### 4.1.1. The Danube Pathway

[31] The obtained extra surface net solar flux in GADSN compared to CTL solely feeds the latent heat flux through an enhanced plant transpiration. Since the increase in the evapotranspiration more than compensates the gain obtained in the solar flux, colder temperatures are observed. Lying nearer to the optimum temperature of the plant activity, they sustain a positive feedback. The modification of the near surface temperature profile, which depends upon the Bowen ratio and locally controls the relative humidity and the degree of instability in the atmosphere, also explains the changes observed in the convective activity and in the cloud cover [see *Schär et al.*, 1999].

#### 4.1.2. The Spain Pathway

[32] Owing to the stronger increase of the surface net solar flux in GADSN, the enhanced plant activity earlier in the growing season soon leads to a severe soil water depletion. The plant stomatal resistance increases, limiting their transpiration capabilities, so that a larger partition of the radiative forcing is used as sensible heat flux and to warm the boundary layer. Warmer temperatures further increase the plant stomatal resistance, leading to the development of a warm and dry climate.

[33] Hence, depending on the atmospheric conditions (e.g., relative humidity), on the vegetation state (the plants are dormant in winter), and on the soil water content, either case (or a combination of them) can develop. Locally, the soil water content acts especially as a limiting factor, e.g., owing to its incomplete recharge at the end of the first year in simulation GADSN.

### 4.2. Sensitivity and Uncertainties

[34] The previously observed and interpreted complex climatic response confirms the nonnegligible role of the aerosols. The increase in the surface net solar flux, the warming over the southern countries, and the enhanced convective activity over some regions obtained in simulation GADSN can be seen as significant. Combined with the numerous uncertainties characterizing aerosol distributions (uncertainties in the atmospheric burden, in the optical parameters, and in the derivation of a radiative forcing, as noted by *IPCC* [2001]), this confirms the need for better scientific understanding, a challenge not only for the simulation of future climate but also for the tuning of those complex tools that are climate and weather models.

[35] In the light of the present results, the use of an inappropriate aerosol distribution is at times contributing to increase (or decrease owing to compensation of model errors) model biases. The well-known cold bias over Spain in CTL may be partly attributed to the too strong desert load in Tanre's climatology. Interpretation is a little more delicate

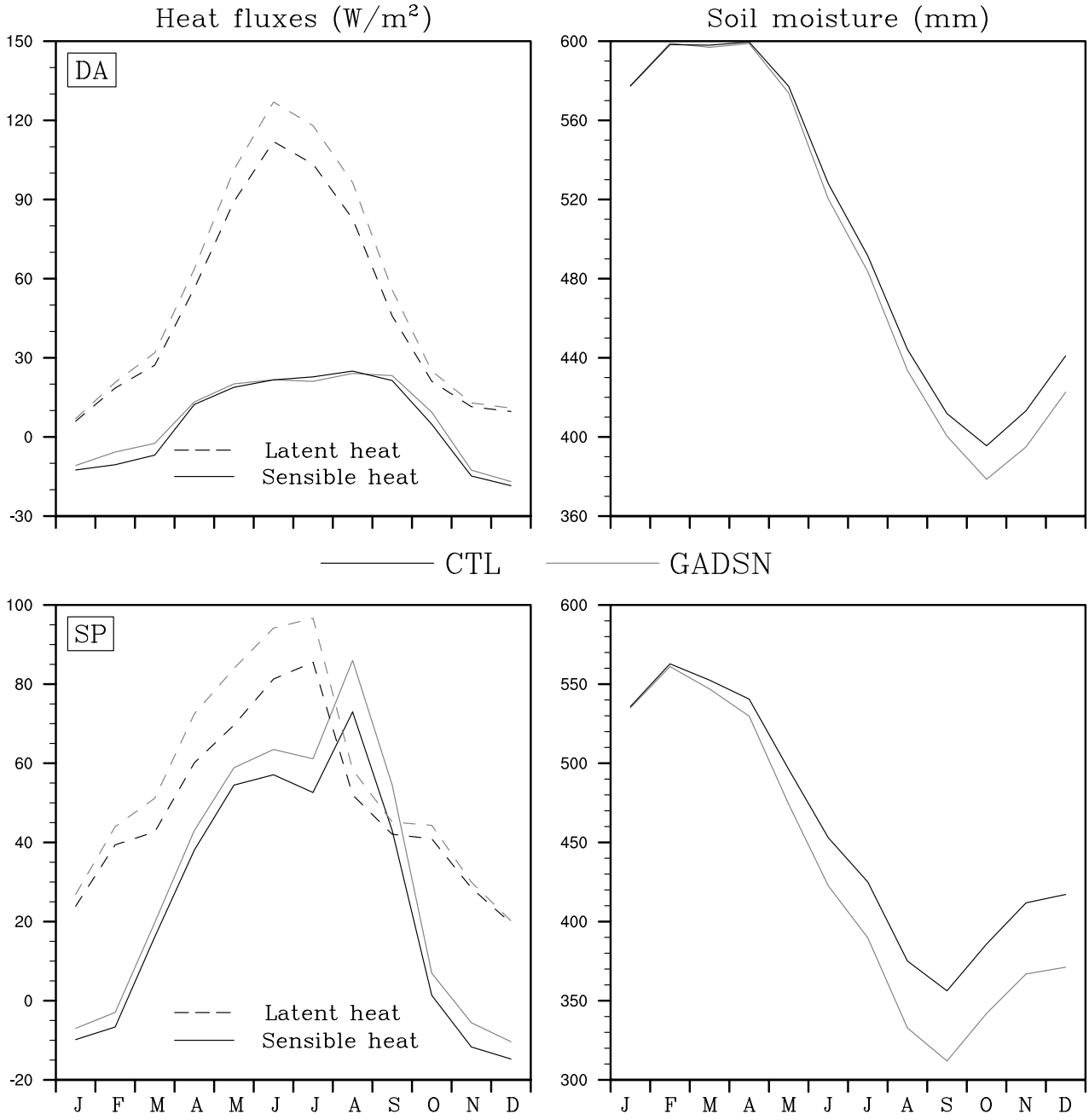


**Figure 13.** Seasonal cycle (1979) of the latent and sensible heat fluxes as well as soil moisture evolution of the simulations CTL and GADSN averaged over the Danube catchment (DA, upper panels) and over Spain (SP, lower panels).

over the Danube region, where the reduction of the summer dry bias in simulation GADSN follows from the soil-atmosphere interactions. The observed increased convective activity can nevertheless be seen as the localized response to the changes brought to the aerosol loading over the Danube region through an enhancement of the evapotranspiration. It also confirms the findings of *Hagemann et al.* [2004], who showed that the summer drying problem of many European models was due to the bias in evapotranspiration and not to the atmospheric transport of moisture into the area.

[36] The best way to assess the impacts of the aerosols on the climate remains the comparison of the calculated aerosol optical depth with its retrieval by satellite (see Figures 1 and 2) and the comparison of the obtained radiative fluxes with observations (as on Figure 7). Both approaches are affected by several uncertainties and restrictions, e.g., quality of measurements, their availability, and the possible compensation of model errors in the simulation of the solar fluxes. Combined with the localized nature of the aerosol forcing, they strongly hamper a thorough validation. Nevertheless, our results seem to indicate that the GADS climatology provides a more realistic estimate of the optical depth of the aerosol particles and thus of their direct radiative forcing than the Tanre data, but due to the

nonconsideration of the indirect effect, it overestimates the observed radiation (at least over Switzerland, see Figure 7). This overestimation is strengthened (damped) in summer (winter) by the use of an invariant aerosol distribution since more (less) aerosols are expected in summer (winter), as could be inferred from the MODIS data (not shown). The characteristic crossing of the GADSN and observational curves on the clear-sky radiance plot of Figure 7 can be clearly interpreted as the footprint of this missing seasonal cycle. The effect is accentuated over mountainous regions where the transport of aerosol particles from the emission sources in the valleys to the mountain tops shows strong temporal variations and thus cannot be resolved with a prescribed aerosol climatology and with our model resolution (smoother topography, see Figure 4). Furthermore, the clear-sky incoming solar flux derived from the ANETZ observations acts rather as a lower limit for the true clear-sky radiance since it is probably still contaminated by some clouds. This is especially the case over the Swiss Plateau in late fall and in winter, when the region lies under persistent fog (almost no cloudless day on Figure 7 in the cold months). In contrast, the excessive "direct" radiative forcing simulated with Tanre's aerosols seems to account for both direct and indirect effects, which may explain the seemingly better solar flux over Switzerland in summer despite unrealistic aerosol distribution on Figure 1.

## 5. Conclusions

[37] An assessment of the sensitivity of the European climate to aerosol forcing has been undertaken using a regional climate model with varying aerosol representations. The first one, still in use in several weather and climate models, was derived by *Tanre et al.* [1984] and appears to be dominated by desert dust over Europe. The second one, based on a modified version of the Global Aerosol Data Set, seems to be better suited to the needs of a RCM with its somewhat higher resolution and its predominance of anthropogenic aerosols over Europe.

[38] The observed changes between the conducted sensitivity experiments can be seen as the result of the modification of the radiation budget through the direct aerosol forcing impacting on the water cycle (which itself impacts on the radiation budget through water vapor and cloud feedbacks) and modifying at the same time the redistribution of energy. While a reduced aerosol optical depth leads to a larger net solar flux at the surface, increased terrestrial emissions, and warmer temperatures, the extra net solar flux can also be used by the plants, augmenting their transpiration, controlling the expected temperature increase, and enhancing convection through boundary layer moist static energy buildup.

[39] The chosen aerosol specification in a RCM appears sufficient to significantly influence the simulated climate over a region and its related biases through complex climatic interactions and feedbacks. The latter speak for the use of a sophisticated aerosol representation in a RCM, e.g., through coupled climate-chemistry models, a point which would need further assessment. However, our results indicate that following a simple approach like updating an aerosol climatology, making use of a higher resolution data set and/or considering seasonally varying 3-D aerosol concentrations, might already improve a RCM performance.

[40] **Acknowledgments.** The support of the ETH Institute for Atmospheric and Climate Science and especially of Christoph Schär was greatly appreciated. This work was funded by the Swiss National Science Foundation (NCCR Climate Project 2.2). The authors wish to acknowledge use of Ferret, NCAR Graphics, GADS, and the ANETZ data provided by the NOAA's Pacific Marine Environmental Laboratory, the University Corporation for Atmospheric Research, the Meteorological Institute of the University of Munich, and MeteoSwiss, respectively. We are also grateful to Reto Stöckli for help with providing MODIS data.

## References

Beljaars, A. C. M., and P. Viterbo (1998), The role of the boundary layer in a numerical weather prediction model, *Clear and Cloudy Boundary Layers*, edited by A. A. M. Holstlag and P. G. Duynkerke, pp. 287–304, R. Neth. Acad. of Arts and Sci., Amsterdam.

Cook, J., and E. J. Highwood (2004), Climate response to tropospheric absorbing aerosols in an intermediate general-circulation model, *Q. J. R. Meteorol. Soc.*, *130*, 175–191.

D'Almeida, G. A., P. Koepke, and E. P. Shettle (1991), *Atmospheric Aerosols: Global Climatology and Radiative Characteristics*, A. Deepak, Hampton, Va.

Dickinson, R. E. (1984), Modeling evapo-transpiration for the three-dimensional global climate models, in *Climate Processes and Climate Sensitivity*, *Geophys. Monogr. Ser.*, vol. 29, pp. 58–72, AGU, Washington, D. C.

Frei, C., J. H. Christensen, M. Déqué, D. Jacob, R. G. Jones, and P. L. Vidale (2003), Daily precipitation statistics in regional climate models: Evaluation and intercomparison for the European Alps, *J. Geophys. Res.*, *108*(D3), 4124, doi:10.1029/2002JD002287.

Gibson, J. K., P. Kallberg, S. Uppala, A. Hernandey, A. Nomura, and E. Serano (1997), ERA description, *ECMWF Reanal. Proj. Rep. Ser.*, vol. 1, 66 pp., Eur. Cent. for Med.-Range Weather Forecasts, Reading, UK.

Gilgen, H., M. Wild, and A. Ohmura (1998), Means and trends of shortwave irradiance at the surface estimated from global energy balance archive data, *J. Clim.*, *11*, 2042–2061.

Giorgi, F., X. Bi, and Y. Qian (2002), Direct radiative forcing and regional climatic effects of anthropogenic aerosols over east Asia: A regional coupled climate-chemistry/aerosol model study, *J. Geophys. Res.*, *107*(D20), 4439, doi:10.1029/2001JD001066.

Giorgi, F., X. Bi, and Y. Qian (2003), Indirect vs. direct effects of anthropogenic sulfate on the climate of east Asia as simulated with a regional coupled climate-chemistry/aerosol model, *Clim. Change*, *58*, 345–376.

Hagemann, S., B. Machenhauer, R. G. Jones, O. B. Christensen, M. Déqué, D. Jacob, and P. L. Vidale (2004), Evaluation of water and energy budgets in regional climate models applied over Europe, *Clim. Dyn.*, *23*, 547–567, doi:10.1007/s00382-004-0444-7.

Haywood, J., and O. Boucher (2000), Estimates of the direct and indirect radiative forcing due to tropospheric aerosols: A review, *Rev. Geophys.*, *38*(4), 513–543.

Hess, M., P. Koepke, and I. Schult (1998), Optical properties of aerosols and clouds: The software package OPAC, *Bull. Am. Meteorol. Soc.*, *79*, 831–844.

Hu, R. M., S. Planton, M. Déqué, P. Marquet, and A. Braun (2001), Why is the climate forcing of sulfate aerosols so uncertain?, *Adv. Atmos. Sci.*, *18*, 1103–1120.

Intergovernmental Panel on Climate Change (IPCC) (2001), *Climate Change 2001: The Scientific Basis, Contribution of Working Group I to the Third Assessment Report of the Intergovernmental Panel on Climate Change*, edited by J. T. Houghton et al., Cambridge Univ. Press, New York.

Jacobsen, I., and E. Heise (1982), A new economic method for the computation of the surface temperature in numerical models, *Contrib. Atmos. Phys.*, *55*, 128–141.

Kaufman, Y. J., D. Tanre, and O. Boucher (2002), A satellite view of aerosols in the climate system, *Nature*, *419*, 215–223.

Kessler, E. (1969), *On the Distribution and Continuity of Water Substance in Atmospheric Circulation Models*, *Meteorol. Monogr.*, vol. 10, Am. Meteorol. Soc., Boston, Mass.

Lin, Y.-L., R. D. Farley, and H. D. Orville (1983), Bulk parameterization of the snow field in a cloud model, *J. Clim. Appl. Meteorol.*, *22*, 1065–1092.

Majewski, D. (1991), The Europa Modell of the Deutscher Wetterdienst, paper presented at Seminar on Numerical Methods in Atmospheric Models, Eur. Cent. for Med.-Range Weather Forecasts, Reading, UK.

Majewski, D., and R. Schrodin (1994), Short description of the Europa-Modell (EM) and Deutschland-Modell (DM) of the Deutscher Wetterdienst (DWD), *Rep. Q. Bull.*, German Weather Serv., Offenbach, Germany.

Mellor, G. L., and T. Yamada (1974), A hierarchy of turbulent closure models for planetary boundary layers, *J. Atmos. Sci.*, *31*, 1791–1806.

New, M., M. Hulme, and P. Jones (1999), Representing twentieth-century space-time climate variability. part I: Development of a 1961–90 mean monthly terrestrial climatology, *J. Clim.*, *12*, 829–856.

Qian, Y., and F. Giorgi (1999), Interactive coupling of regional climate and sulfate aerosol models over eastern Asia, *J. Geophys. Res.*, *104*(D6), 6477–6499.

Qian, Y., L. R. Leung, S. J. Ghan, and F. Giorgi (2003), Regional climate effects of aerosols over China: Modeling and observation, *Tellus, Ser. B*, *55*, 914–934.

Ritter, B., and J. Geleyn (1992), A comprehensive radiation scheme for numerical weather prediction models with potential applications in climate simulations, *Mon. Weather Rev.*, *120*, 303–325.

Schär, C., D. Lüthi, U. Beyerle, and E. Heise (1999), The soil-precipitation feedback: A process study with a regional climate model, *J. Clim.*, *12*, 722–741.

Sellers, P. J., C. J. Tucker, G. J. Collatz, S. O. Los, C. O. Justice, D. A. Dazlich, and D. A. Randall (1994), A global 1-degrees by 1-degrees NDVI data set for climate studies. part 2: The generation of global fields of terrestrial biophysical parameters from the NDVI, *Int. J. Remote Sens.*, *15*, 3519–3545.

Tanre, D., J. F. Geleyn, and J. Slingo (1984), First results of the introduction of an advanced aerosol-radiation interaction in the ECMWF low resolution global model, in *Aerosols and Their Climatic Effects: Proceedings of the Meetings of Experts, Williamsburg, Va., 28–30 March 1983*, edited by H. E. Gerber and A. Deepak, pp. 133–177, A. Deepak, Hampton, Va.

Tanre, D., F. M. Bréon, J. L. Deuze, M. Herman, P. Goloub, F. Nadal, and A. Marchand (2001), Global observation of anthropogenic aerosols from satellite, *Geophys. Res. Lett.*, *28*(24), 4555–4558.

Tegen, I., P. Hollrig, M. Chin, I. Fung, D. Jacob, and J. Penner (1997), Contribution of different aerosol species to the global aerosol extinction optical thickness: Estimates from model results, *J. Geophys. Res.*, *102*(D20), 23,895–23,915.

Tiedtke, M. (1989), A comprehensive mass flux scheme for cumulus parameterization in large-scale models, *Mon. Weather Rev.*, *117*, 1779–1800.

Vidale, P., D. Lüthi, C. Frei, S. I. Seneviratne, and C. Schär (2003), Predictability and uncertainty in a regional climate model, *J. Geophys. Res.*, *108*(D18), 4586, doi:10.1029/2002JD002810.

Wang, C. (2004), A modeling study on the climate impacts of black carbon aerosols, *J. Geophys. Res.*, *109*(D3), D03106, doi:10.1029/2003JD004084.

World Climate Research Program (1980), Aerosols and climate, *Rep. WCP-12*, Int. Counc. of Sci. Unions, World Meteorol. Org., Geneva.

Wu, J., W. M. Jiang, C. B. Fu, B. K. Su, H. N. Liu, and J. P. Tang (2004), Simulation of the radiative effect of black carbon aerosols and the regional climate responses over China, *Adv. Atmos. Sci.*, *21*, 637–649.

C. Hohenegger, Institute for Atmospheric and Climate Science, ETH, Winterthurerstr. 190, 8057 Zürich, Switzerland. (cathy.hohenegger@env.ethz.ch)

P. L. Vidale, National Environment Research Council Centres for Atmospheric Science, Centre for Global Atmospheric Modeling, University of Reading, Earley Gate, Reading RG6 6BB, UK. (p.l.vidale@reading.ac.uk)